



Research Article

## Second law analysis on an elliptical twisted tube for a heat exchanger

Toygun DAGDEVIR<sup>1\*</sup>

<sup>1</sup>Department of Mechanical Engineering, Erciyes University, Kayseri, Turkey

### ARTICLE INFO

*Article history*

Received: 22 July 2021

Accepted: 28 September 2021

**Keywords:**

Second Law Analysis; Entropy Generation; Irreversibility; Heat Transfer Enhancement; Elliptical Twisted Tube

### ABSTRACT

This work presents a second law analysis on a heat exchanger tube configured as circular smooth tube (CST), elliptical smooth tube (EST) and elliptical twisted tube (ETT) with different aspect ratios and pitch lengths. The ETTs were configured with different aspect ratio (AR) of 1.5 and 2.0 and twist pitch length (PL) of 50, 100 and 200 mm. The hydraulic diameter was kept as constant for all cases, since the results are influenced by the change in hydraulic diameter. CFD analyzes were run to perform the second law analysis of the considered cases. The analyzes were carried out by considering that the thermo-physical properties of the water fluid change depending on the temperature. Besides, the analyzes were carried out under steady state condition and turbulent flow condition which corresponds to Reynolds number ranging from approximately 4000 to 27,000. The results are evaluated and discussed in terms of the thermal, the frictional and the total entropy generation, the Bejan number, the entropy generation number, the exergy destruction and the second law efficiency. It is resulted that the increase in AR and the decrease in PL for the ETTs show better the second law efficiency. As a result, in the case of ETT\_AR=2.0\_PL=50 at the minimum mass flow rate considered in the study, the highest second law efficiency is obtained as 0.45, which corresponds to a value greater than 80% in the case of CST.

**Cite this article as:** Toygun D. Second law analysis on an elliptical twisted tube for a heat exchanger. J Ther Eng 2022;8(3):349–362.

### INTRODUCTION

Due to the rapidly increasing energy consumption, the efficient use of energy has been a significant issue in recent years. Improving the performance of thermal devices such as heat exchangers, heat pipes and refrigerators is critical for energy savings. Various techniques have been investigated and applied to enhance the heat transfer performance of the thermal devices. These techniques are basically divided into

two as active and passive techniques. While the active techniques demand extra power input to the system [1–3], the passive technique is performed with no extra power input methods such as inserting turbulator devices (twisted tapes [4–9], coiled wires [10–13], helical tapes [14,15], nozzles [16]) into the heat pipe, surface modification of the heat pipe [17,18], modifying the heat pipe (coiled tube [19],

\*Corresponding author.

\*E-mail address: [toygun@erciyes.edu.tr](mailto:toygun@erciyes.edu.tr)

*This paper was recommended for publication in revised form by Regional Editor Muslum Arici*



twisted tube [20–22]) and using nanofluids for the working fluid [23–27] etc.

Farnam et al. [28] investigated the effect of the use of twisted tube and the twisted tape inserted in a U-tube heat exchanger on the heat transfer augmentation. They reported that the case of twisted tube equipped by twisted tape having lower twist ratio gives the highest performance at the lowest Reynolds number considered in their study. Dong et al. [22] used a spiral twisted tube heat exchanger to investigate the heat transfer and flow resistance. They recommended that the use of the spiral twisted tube in a heat exchanger is a good choice for both laminar and turbulent flows. Thantharate and Zodpe [29] experimentally and numerically compared a twisted tube with a plain tube with respect to heat transfer performance. They revealed that the use of twisted tube is beneficial for high Reynolds number, but not for low flow rates. Tan et al. investigated the thermohydraulic performance of a heat exchanger including twisted oval tube. They concluded that the twisted oval tube showed effective performance for using in a heat exchanger. Wang et al. [30] experimentally and numerically investigated the thermohydraulic performance of the heat exchanger equipped helically coiled-twisted trilobal in the tube side. They concluded that the helically coiled twisted trilobal tube showed better thermohydraulic performance than the helically coiled plain tube. Shahsavar et al. [31] numerically investigated the effect of twisted tube with nanofluid on the hydrothermal performance of double-pipe heat exchanger. As a result of their investigation, they reported that the use of twisted double-pipe heat exchanger showed better performance than plain double-pipe heat exchanger. Sun et al. [32] conducted an experimental study on the built-in twisted belt external thread tubes flowing various nanofluids. They concluded that the built-in twisted belt external thread tube provided better thermal performance than horizontal tube.

In addition to thermohydraulic performance investigations, a few second law analyzes, consisting of entropy and exergy analysis, were performed on the heat exchangers by using passive techniques [33–36]. Bahiraei et al. [37] researched the double twisted tape inserted tube flowing hybrid nanofluid in terms of second law analysis. They resulted that the used of the double counter twisted tapes provided lower entropy than that of the double co-twisted tapes. Naphon [38] investigated the effect of flow rate and fluid temperature for the horizontal concentric tube heat

exchanger on the second law. Dizaji et al. [39] presented a comprehensive study on second law analysis of a tube-in-tube helically coiled heat exchangers. They concluded that the effect of coil pitch was negligible on exergy loss. Khanmohammadi and Mazaheri [40] investigated that second law analysis of single and double twisted tape inserted tube. They resulted that double twisted tape showed better exergy destruction rate and second law efficiency than single twisted tape. Sheikholeslami et al. [41] investigated the second law analysis on helical swirl flow device inserted into the tube flowing CuO-H<sub>2</sub>O nanofluid. Mwesigye et al. [42] investigated that entropy generation analysis of parabolic solar collector with using Cu-Therminol®VP-1 nanofluid. They concluded that the entropy generation rate decreased up to 30% at the flow rate of 45 m<sup>3</sup>/h. Entropy generation analysis of water based magnetite nanofluid in a circular microtube with twisted porous blocks is carried out by Ibrahim et al. [43]. They reported that the use of twisted porous blocks increased the heat transfer and entropy generation owing to the reduced thermal boundary thickness.

As mentioned in the literature review, significant researches have been conducted on second law analyzes of various heat exchange tube configurations. However, a comprehensive second law analysis which includes the thermal, the frictional and the total entropy generation, the Bejan number, the entropy generation number, the exergy destruction and the second law efficiency has not been presented on elliptical twisted tube with various aspect ratios and pitch lengths, yet. Therefore, the main objective and the originality of the present study is comprehensively to investigate the elliptical twisted tubes having various aspect ratios and twist pitch lengths by considering the second law parameters.

## MATERIAL AND METHODOLOGY

### Physical Model

In this work, numerical analyzes are conducted to investigate the second law analysis of circular smooth tube (CST), elliptical smooth tube (EST) and elliptical twisted tube (ETT). Boundary condition types adopted for the solution domain are depicted in Figure 1. The ETTs are configured with different aspect ratios (AR) of 1.5 and 2.0 and twist pitch lengths (PL) of 50, 100 and 200 mm. The cases of the considered tubes are illustrated in Fig. 2. The dimensions of the ellipse (a and b) are adjusted so that the

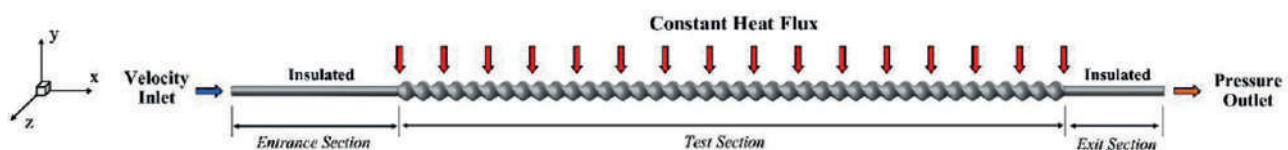


Figure 1. Solution domain adopted in the study.

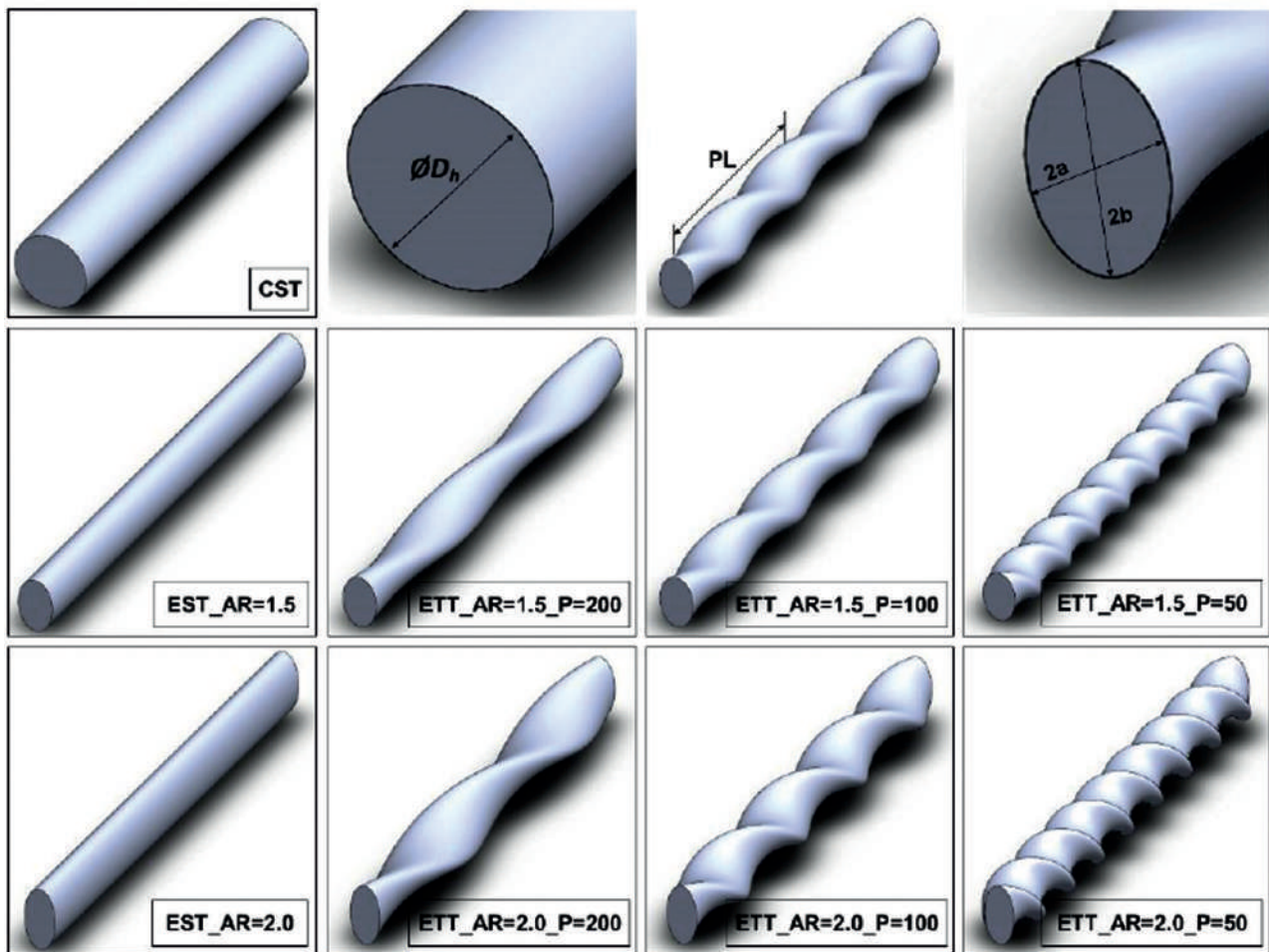


Figure 2. Tube configurations considered in the study.

Table 1. Boundary conditions assumed in the study

Boundary name	Boundary type	Boundary condition	Dimension
Inlet	Velocity inlet	Velocity magnitude calculated with $Re$ , normal to boundary	Hydraulic diameter of 17 mm
Entrance section	Wall	No-slip and adiabatic	Length of 250 mm
Test section	Wall	No-slip and constant heat flux of $50 \text{ kW/m}^2$	Length of 1000 mm
Exit section	Wall	No-slip and adiabatic	Length of 150 mm
Outlet	Pressure outlet	Gauge pressure of 0 Pa, normal to boundary	Hydraulic diameter of 17 mm

hydraulic diameter of 17 mm is constant. Thus, the results of the analyzes could be examined independently of the hydraulic diameter. The boundary conditions adopted in the study are summarized in Table 1.

In order to provide the turbulent fully developed flow condition, an entrance tube with length of 250 mm which is  $L_e/D \geq 10$  is placed before the test section, as stated in a book by Cengel and John [44]. Fig. 3 shows the development of the flow from inlet to the test section. It can be seen

that the velocity vectors are developed, as the fluid flows through the tube. Since the velocity profiles become stable before the test section where  $x/D=14.70$ , the length of the entrance section was found to be sufficient to obtain fully developed flow. In addition, velocity magnitudes belong to various  $x/D$  locations are given in Fig. 3b. It is also seen that the velocity profile in the test section has same magnitude which is another proof for ensuring the developed flow condition on the test section. An exit section with a length

of 150 mm is placed to prevent the reserve flow effects by the twisted surfaces.

**Numerical Method**

Heat transfer performance and flow characteristic of the considered tubes are numerically investigated by using Ansys-Fluent version of 18.0 as a CFD program. The analyses are conducted under steady state condition. Inlet temperature of the fluid is selected as 300 K. Various mass flow rates ranging from 0.040kg/s to 0.266 kg/s which correspond to turbulent flow conditions are applied on the numerical analyzes. A constant heat flux of 50 kW/m<sup>2</sup> is applied onto the test section. The thermophysical properties of water selected as the working fluid are taken into account with the change in temperature of the fluid as adopted in the studies [45–47]. The properties are imported to the CFD program as a polynomial function as given in Eq. (1). Each function is generated with curve fitting by using STATISTICA software with regression value of at least 0.999%. The coefficients of the functions for each property are given in Table

2. The walls of the all tubes are taken into account of non-slip boundary condition, while the walls of the tubes on the entrance and exit sections are taken into account of insulated boundary condition. Standard k- $\omega$  turbulence model is selected for the numerical analyzes considered in the study as studies by researchers [48][49][50]. A careful mesh independence check is performed as given in Fig. 4. As a result, a mesh structure having number of cells of approximately 2.4 million is selected, because the results of the  $Nu$  and the  $f$  are not respectively affected more than 0.46% and 3.96%, even if the number of cell increases from this value. Finally, polyhedral mesh structure with boundary layer mesh which has  $y^+$  of averagely 1.68, is adopted for the solution domain, as shown in Figure 5.

$$f(T) = a + bT + cT^2 + dT^3 \tag{1}$$

**Governing Equations**

Conservation of continuity (2), momentum (3) and energy (4) equations are solved by the CFD program. SIMPLE algorithm scheme is used to obtain pressure field and to enforce mass conservation by achieving the relationship between pressure and velocity coupling [51]. Convergence criteria of the solutions are defined as  $1 \times 10^{-5}$  for continuity, velocities, k and  $\omega$  and  $1 \times 10^{-7}$  for energy.

$$\nabla(\rho\vec{V}) = 0 \tag{2}$$

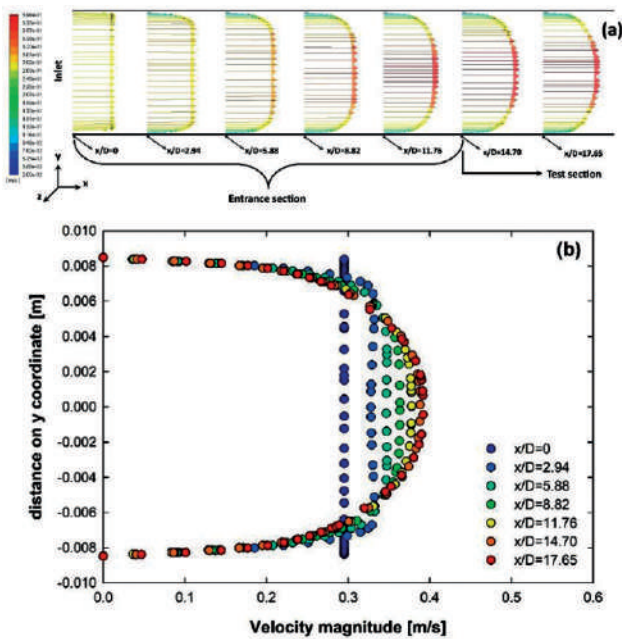


Figure 3. (a) Velocity vector and (b) velocity profiles through the tube at Reynolds number of 6459.

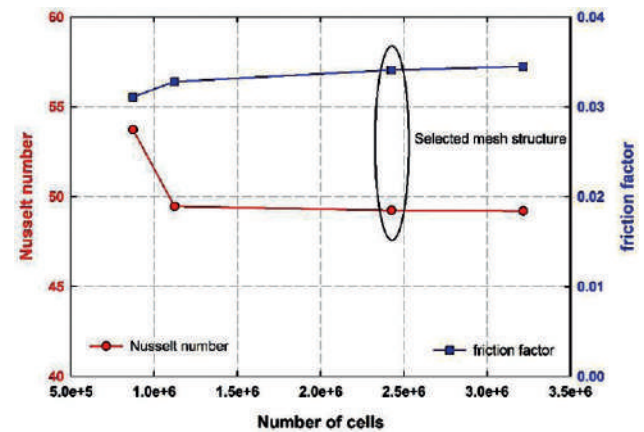


Figure 4. Mesh independence check results.

Table 2. Coefficient of the functions of the thermophysical property of the working fluid used in the study

Thermophysical properties	a	b	c	d
$\rho$ [kg/m <sup>3</sup> ]	719.22	2.29643	-5.15027E-3	1.90856E-6
$c_p$ [j/kgK]	6217.4	-15.2458	3.52006E-2	-2.33218E-5
k [W/mK]	-1.33612	1.29259E-2	-2.6746E-5	1.76382E-8
$\mu$ [kg/ms]	0.0597994	-4.73471E-4	1.26033E-6	-1.2233E-9

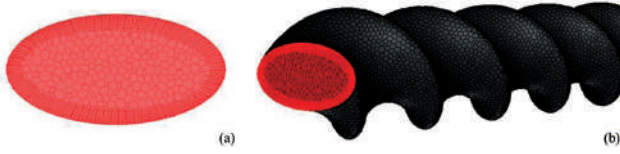


Figure 5. Mesh structure used for the numerical analysis.

$$\nabla(\rho\bar{V}\bar{V}) = -\Delta P + \nabla(\mu\nabla\bar{V}) \quad (3)$$

$$\nabla(\rho C_p \bar{V}T) = \nabla(k\nabla T) \quad (4)$$

**Data Reduction**

Parameters used in the study are calculated with exporting from the CFD program with area-weighted average by using surface integrals. Reynolds number ( $Re$ ), Nusselt number ( $Nu$ ) and friction factor ( $f$ ) are expressed as in Eq. (5), Eq. (6) and Eq. (9), respectively. Besides, the  $Nu$  is calculated with using Eq. (7) and Eq. (8).  $T_s$  and  $T_b$  represent the temperature of the wall surface of the test section and the bulk temperature between inlet and outlet through the test section, respectively.

$$Re = \frac{\rho D_h V}{\mu} \quad (5)$$

$$Nu = \frac{h D_h}{k} \quad (6)$$

$$h = \frac{q''}{\Delta T} \quad (7)$$

$$\Delta T = T_s - T_b \quad (8)$$

$$f = \frac{\Delta P}{\frac{1}{2}\rho V^2 \frac{L}{D_h}} \quad (9)$$

**Second Law Analysis**

Definition of the first law efficiency cannot be sufficient to evaluate the engineering systems and lead to misinterpretations. Therefore, the second law analysis is evaluated for the engineering systems to remedy this deficiency [52]. Entropy generation defined in the second law is calculated for the heat exchanger as in the followings [53]. Total entropy generation ( $\dot{S}'_{gen,total}$ ) is the sum of the irreversibilities by heat transfer and friction as defined in Eq. 10. The thermal entropy generation ( $\dot{S}'_{gen,th}$ ) and the frictional entropy generation ( $\dot{S}'_{gen,f}$ ) in the 3D numerical form are determined as in Eq. (11) and Eq. (12), respectively. Global entropy generation rate ( $\dot{S}$ ) in the 3D solution domain is expressed with Eq. (13) by integrating the local entropy generation rates [40].

$$\dot{S}'_{gen,total} = \dot{S}'_{gen,th} + \dot{S}'_{gen,f} \quad (10)$$

$$\dot{S}'_{gen,th} = \frac{k}{T^2} \left[ \left( \frac{\partial T}{\partial x} \right)^2 + \left( \frac{\partial T}{\partial y} \right)^2 + \left( \frac{\partial T}{\partial z} \right)^2 \right] \quad (11)$$

$$\dot{S}'_{gen,f} = \frac{\mu}{T} \left\{ 2 \left[ \left( \frac{\partial V_x}{\partial x} \right)^2 + \left( \frac{\partial V_y}{\partial y} \right)^2 + \left( \frac{\partial V_z}{\partial z} \right)^2 \right] + \left( \frac{\partial V_x}{\partial y} + \frac{\partial V_y}{\partial x} \right)^2 + \left( \frac{\partial V_x}{\partial z} + \frac{\partial V_z}{\partial x} \right)^2 + \left( \frac{\partial V_y}{\partial z} + \frac{\partial V_z}{\partial y} \right)^2 \right\} \quad (12)$$

$$\dot{S} = \int \dot{S}' dV \quad (13)$$

The ratio of the entropy generation rate of the elliptical tubes with and without twist to that of CST is called as entropy generation number ( $N_s$ ) and defined as in Eq. (14). The  $N_s$  is desired as lower than 1.0 for heat transfer enhancement applications.

$$N_s = \frac{\dot{S}_{gen,ET}}{\dot{S}_{gen,CST}} \quad (14)$$

Bejan number ( $Be$ ) is used to evaluate the relatively contribution of the thermal and the frictional entropy generation. In other words, the  $Be$  is defined as the ratio of thermal entropy generation rate to the total entropy generation rate, as in Eq. (15). The Eq. (16), (17) and (18) define the imported exergy ( $X_q$ ), the exergy destruction ( $X_d$ ) and the second law efficiency ( $\eta$ ), respectively [40].

$$Be = \frac{\dot{S}_{gen,th}}{\dot{S}_{gen,total}} \quad (15)$$

$$X_q = q'' A \left( 1 - \frac{T_0}{T_s} \right) \quad (16)$$

$$X_d = \dot{m} c_p (T_{in} - T_{out}) + \dot{m} c_p T_0 \ln \left( \frac{T_{out}}{T_{in}} \right) + X_q \quad (17)$$

$$\eta = \frac{x_q - x_d}{x_q} \quad (18)$$

**Validation of Numerical Methodology**

Validation of the numerical methodology is presented in Fig. 4, by comparing the results of the  $Nu$  and the  $f$  versus the  $Re$  for the case of the CST with the correlations in the literature. Gnielinski Eq. (19) [54] and Blasius Eq. (20) [55] are used to compare the results of the study according to the  $Nu$  and the  $f$ , respectively. The limits of the parameters used

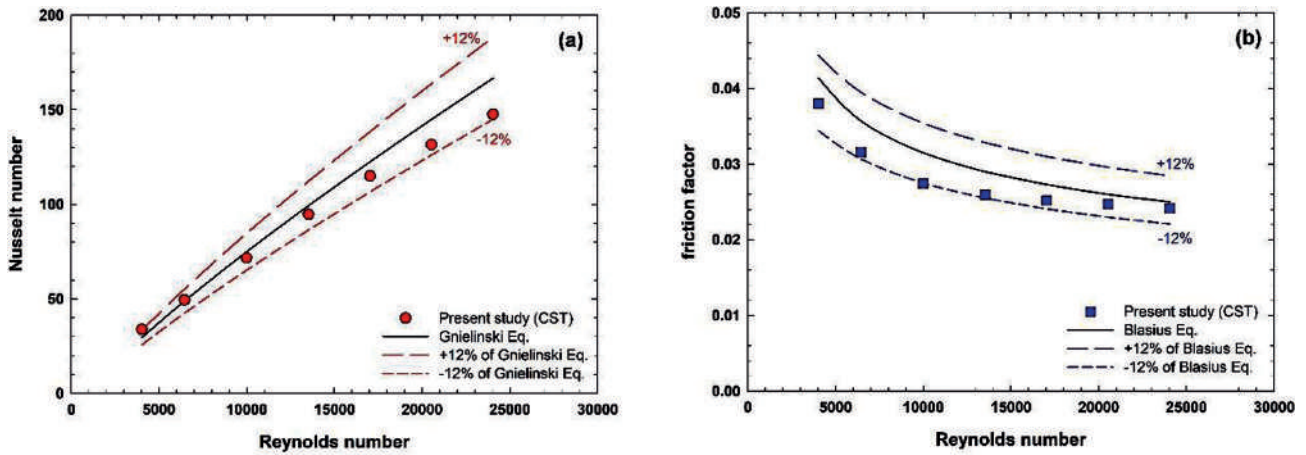


Figure 6. Comparison of the results of the case of CST for a) the  $Nu$  and b) the  $f$  versus the  $Re$ .

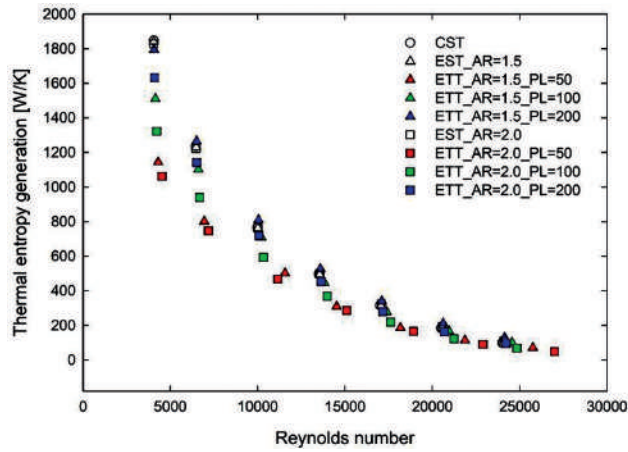


Figure 7. Distribution of the thermal entropy generation rates versus Reynolds number.

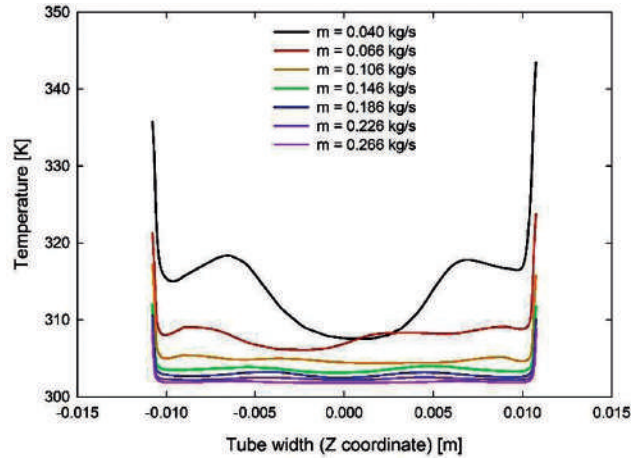


Figure 8. Temperature profiles at  $x/D=61.76$  of the case of  $ETT\_AR=1.5\_PL=50$  for various mass flow rates.

in the present study such as according to  $Re$ ,  $Pr$  and  $L/D$  are within the valid range of the equations used for the validation. As shown in Fig. 6, the maximum deviations of the  $Nu$  and the  $f$  results with the literature are respectively within +11.28% and -11.96%, where they are in acceptable range.

$$Nu = \frac{(f/8)(Re - 1000)Pr}{1 + 12.7(f/8)^{1/2}(Pr^{2/3} - 1)} \quad 3000 \leq Re \leq 5 \times 10^6, \quad 0.5 \leq Pr \leq 2000, \quad \frac{L}{D} \geq 10 \quad (19)$$

$$f = 0.316Re^{-0.25} \quad Re \leq 2 \times 10^4 \quad (20)$$

## RESULTS AND DISCUSSION

### Second Law Analysis

The second law analysis performed in this study is evaluated by considering the following parameters.

- Thermal entropy generation ( $\dot{S}_{gen,th}'''$ ),
- Frictional entropy generation ( $\dot{S}_{gen,f}'''$ ),
- Total entropy generation ( $\dot{S}_{gen}'''$ ),
- Bejan number ( $Be$ ),
- Entropy generation number ( $N_s$ ),
- Exergy destruction ( $X_d$ )
- Second law efficiency ( $\eta$ ).

### Thermal Entropy Generation

Fig. 7 shows the distribution of the thermal entropy generation rates with respect to  $Re$ . It is clearly seen that the trend of the thermal entropy generation rates tends to decrease with the increment of the  $Re$ , since the bulk temperature through the tube decreases. Fig. 8 is given to show the temperature profiles of the case of  $ETT\_AR=1.5\_PL=50$  with respect to the mass flow rates. The decrement of the bulk temperature is clearly seen from the Fig. 8 with the increment of the mass flow rate, corresponding to related

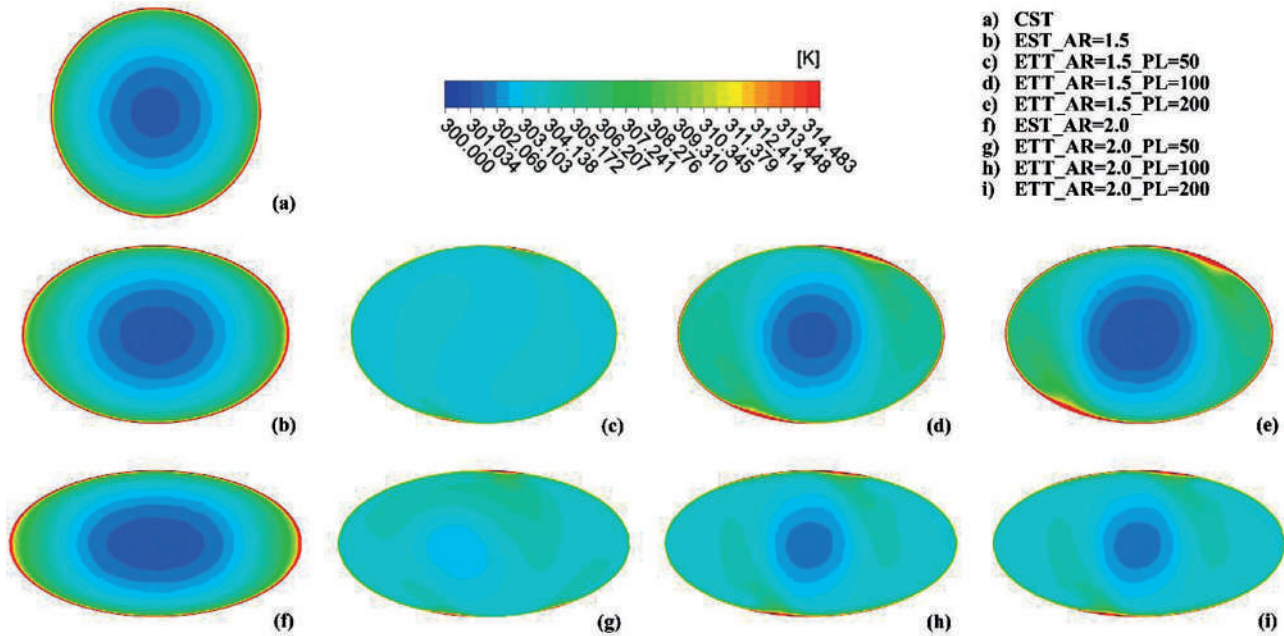


Figure 9. Temperature contours for the considered tubes at  $x/D=61.76$  and mass flow rate of  $0.146 \text{ kg/s}$ .

*Re*. Furthermore, as the mass flow rate increases, the thermal entropy generation decreases, because the temperature profiles become smoother and the irreversibility reduces.

One of the main investigated issues of the present study is second law analysis of different twisted tube configurations having various aspect ratios (AR) and twist pitch lengths (PL). Fig. 7 also shows the relationship among the AR and PL in terms of thermal entropy generation. The thermal entropy generation rates decrease with the increment of AR and the decrement of PL. On one hand, the thermal boundary layer becomes thinner, as the AR increases. The temperature contours of the considered tube configurations at  $x/D=61.76$  are given in Fig. 9. It is clearly seen from the figure that the cases of the ETTs have greater bulk temperature than the ESTs and the CST. Furthermore, it can be stated that if the temperature magnitude on the surface of the tube is higher, there is no effective heat transfer from the wall to the fluid. The bulk temperature of the fluid increases, as the AR increases and the PL decreases. As result, the case of ETT\_AR=2.0\_PL=50 shows the most effective heat transfer performance, since the bulk temperature of the fluid is the highest and the wall temperature is the lowest compared to other cases.

On the other hand, as the PL decreases, the flow more efficiently mixes through the tube and it leads to get more uniform temperature profile. These two phenomena provide that the heat from the heated wall to the fluid transfers more efficiently. The temperature profiles for the considered tube configurations are given in Fig. 10 which supports these results. In brief, the smoothing of the temperature profiles at the tube cross-section and the decrease in the

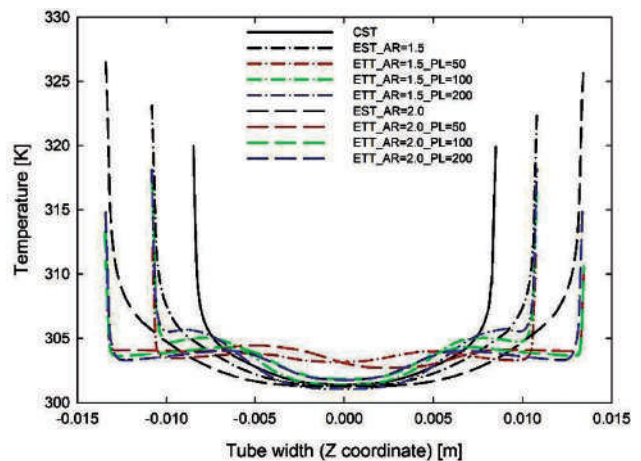


Figure 10. Temperature profiles for the considered tubes at  $x/D=61.76$  and mass flow rate of  $0.146 \text{ kg/s}$ .

temperature of the fluid lead to decrease in the thermal entropy generation.

### Frictional Entropy Generation

Distribution of the frictional entropy generation rates as a function of the *Re* is given in Fig. 11. In contrast to the thermal entropy generation, the frictional entropy generation increases with the increment of the *Re*. Reason of this result is that the increase in the velocity gradient through the tube wit the increment of the *Re* increases the irreversibility. The relationship between the velocity profile and the

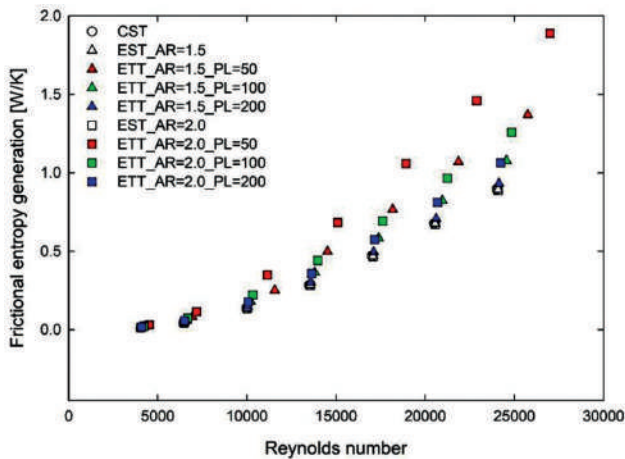


Figure 11. Distribution of frictional entropy generation results versus Reynolds number.

mass flow rate for the case of ETT\_AR=1.5\_PL=50 among is given in Fig. 12. As a result, the frictional entropy generation increases, as the mass flow rate increases due to increase in the irreversibility.

Moreover, the Fig. 13 shows the velocity profiles for the considered tube configurations at mass flow rate of 0.146. It is seen from the figure that the more the velocity gradient intensifies, as the AR increases and PL decreases. As known, “U” velocity profile occurs for the developed flow through the circular smooth tube (CST) as shown in Fig. 13. Irregularity in the velocity profile indicates the occurrence of the secondary flow. The secondary flow characteristics of the EST and the ETT are seen from the Fig. 14. The larger the intensity of the secondary flow velocity becomes, the greater the frictional entropy generation occurs. Particularly, the highest distribution on the velocity profile is observed from the case of ETT\_AR=2.0\_PL=50. This is the result of the fact that highest frictional entropy generation is observed from the case of ETT\_AR=2.0\_PL=50, as shown in Fig. 11. As a result, the utilization of twisted tube with a high AR and a low PL is not beneficial in terms of the frictional entropy generation.

### Total Entropy Generation

Distribution of the total entropy generation results versus  $Re$  is given in Fig. 15. The total entropy generation tends to decrease with the increment of Reynolds number. The trend of the total entropy generation is similar to the that of the thermal entropy generation, because the thermal entropy generation is more dominant rather than the frictional entropy generation. The total entropy generation results of the considered tube configurations become very close each other when the maximum Reynolds number is reached. The lowest total entropy generation is observed for the case of ETT\_AR=2.0\_PL=50 at maximum considered

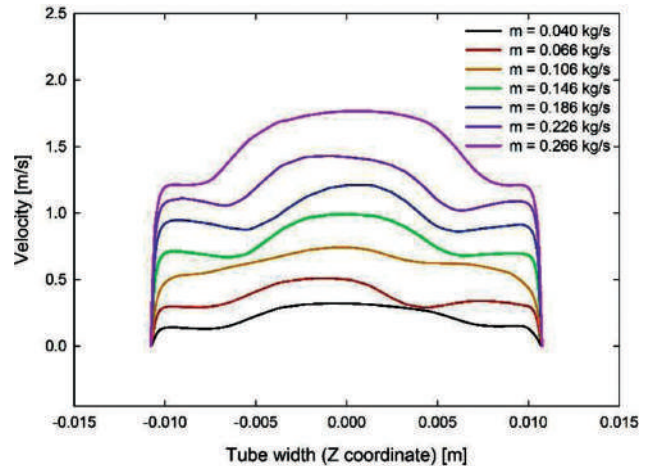


Figure 12. Velocity profiles at  $x/D = 61.76$  of the ETT\_AR = 1.5\_PL = 50 for various mass flow rates.

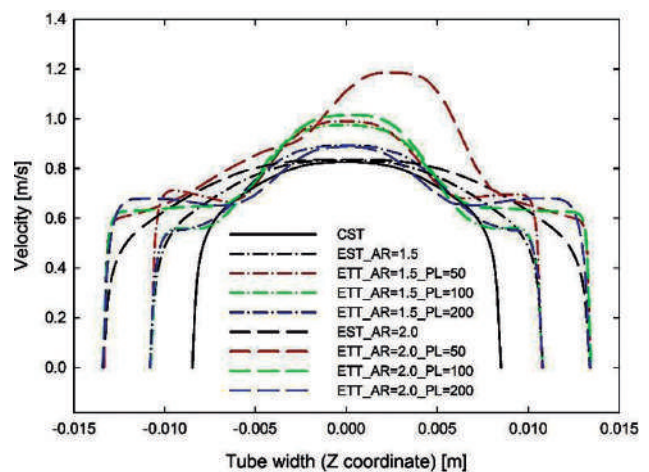


Figure 13. Velocity profiles for the considered tubes at  $x/D = 61.76$  and mass flow rate of 0.146.

the mass flow rate of 0.266 kg/s, corresponding to Reynolds number of 26,998. It is resulted that a better performance in terms of total entropy generation is obtained as the AR increases and the PL decreases for the elliptical twisted tube.

### Bejan Number

Distribution of Bejan number ( $Be$ ) that is a definition of the ratio of thermal entropy generation rate to the total entropy generation rate, with respect to the  $Re$  is plotted in Fig. 16. The  $Be$  has a decreasing trend, as the  $Re$  increases. It is seen from the figure that the frictional entropy generation rate has greater influence at higher  $Re$ , especially for the case of ETT\_AR=2.0\_PL=50 which has the highest friction factor.

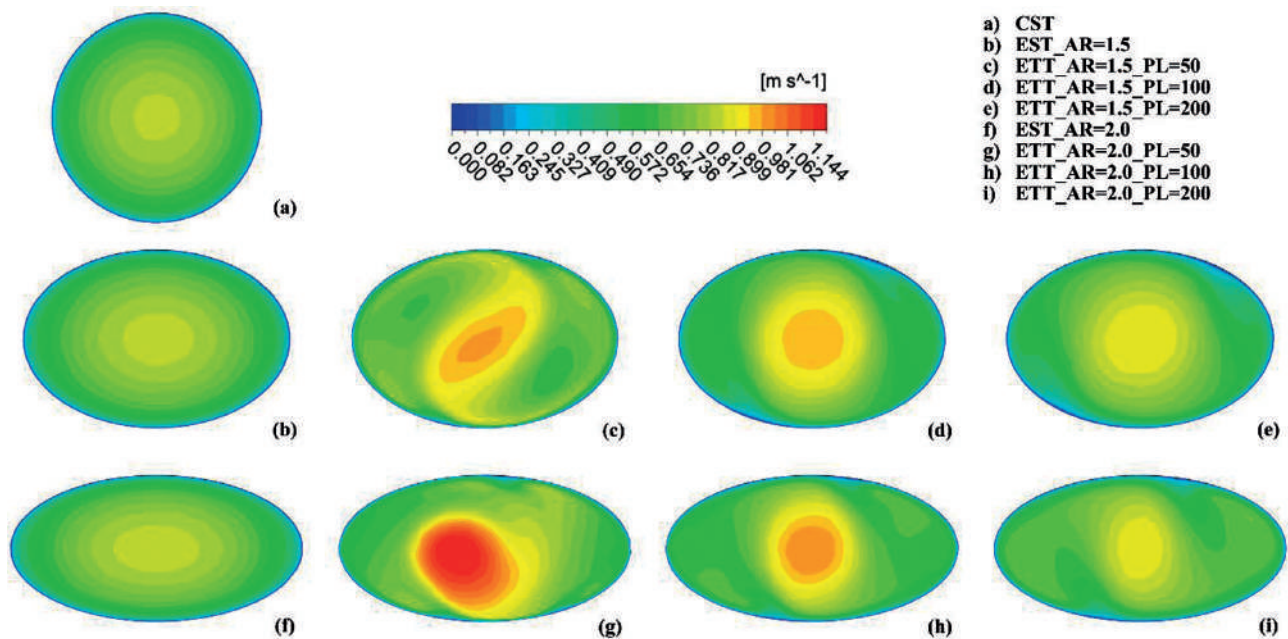


Figure 14. Velocity contours for the considered tubes at  $x/D = 61.76$  and mass flow rate of  $0.146 \text{ kg/s}$ .

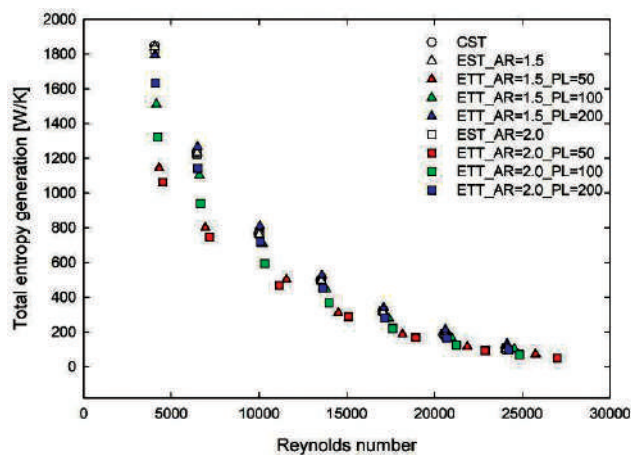


Figure 15. Distribution of total entropy generation results versus Reynolds number.

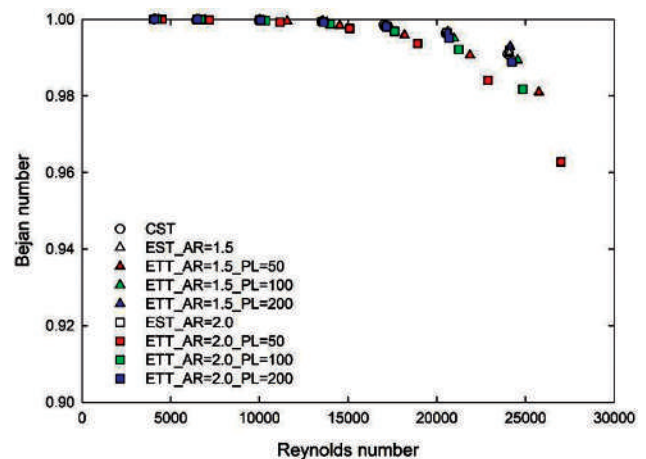


Figure 16. Distribution of Bejan number versus Reynolds number.

### Entropy Generation Number

Fig. 17 shows the results of entropy generation number ( $N_s$ ) versus the  $Re$ . Although a significant change in the  $N_s$  is not observed in the range of the  $Re$  considered in the study, the  $N_s$  belongs to the case of  $ETT\_AR=1.5\_PL=200$  increases with the increment of the  $Re$ . The cases with the  $N_s$  value less than 1.0 value are thermodynamically beneficial for the application. Especially, the case of  $ETT\_AR=2.0\_PL=50$  shows the best performance, because of presenting the lowest  $N_s$  ranging from 0.49 to 0.61. In the other hand, better  $N_s$  results are obtained, as the AR increases and the PL decreases in the elliptical twisted tube.

### Exergy Destruction

Fig. 18 shows the distribution of exergy destruction ( $X_d$ ) results versus the  $Re$ . The results of the  $X_d$  have similar trend with the those of the total entropy generation. The result of the  $X_d$  for the case of CST is higher than those of the elliptical tubes. It means that the heat from wall to the fluid is not efficiently transferred by CST compared to other tubes. The lowest  $X_d$  which means the most effective heat transfer is observed by the case of  $ETT\_AR=2.0\_PL=50$  at mass flow rate of  $0.266 \text{ kg/s}$ , corresponding to Reynolds number of 26,998. When the relationship between the  $X_d$  and the AR and PL of the twisted tube is considered, it is recommended

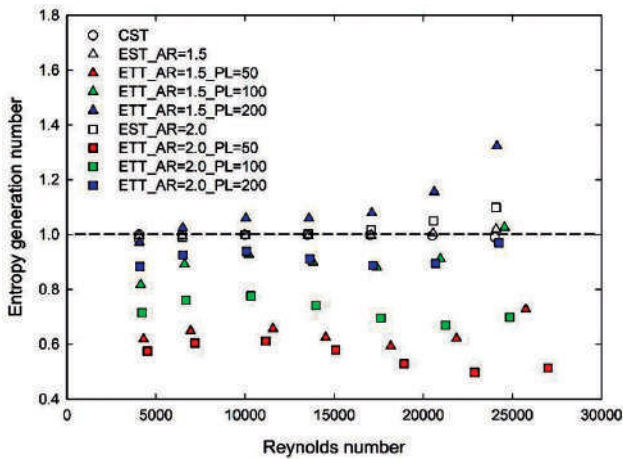


Figure 17. Distribution of entropy generation number results versus Reynolds number.

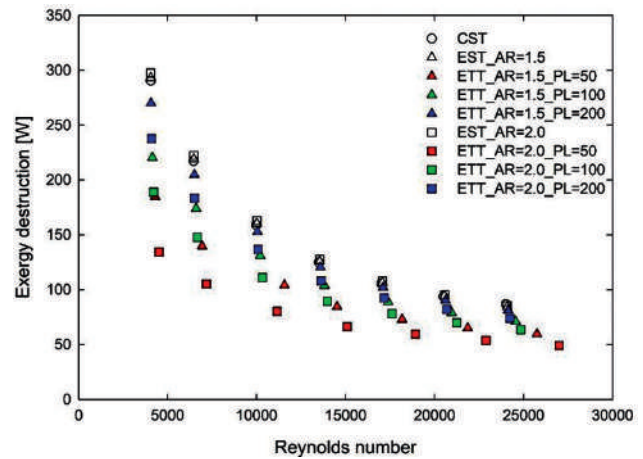


Figure 18. Distribution of exergy destruction results versus Reynolds number.

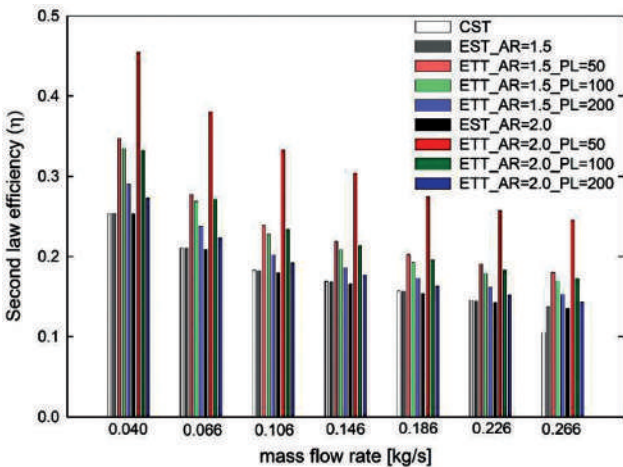


Figure 19. Distribution of second law efficiency results versus mass flow rate.

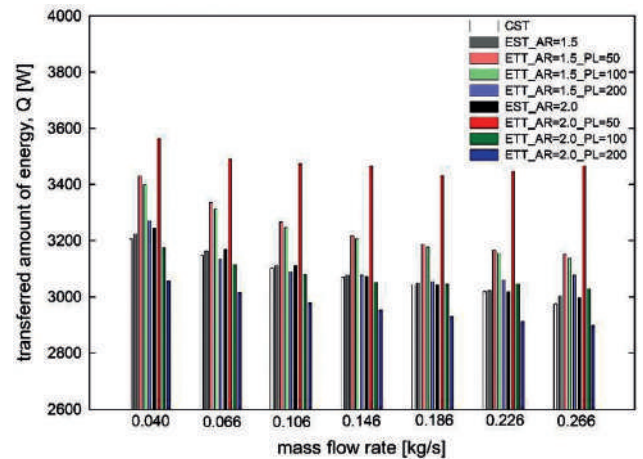


Figure 20. Distribution of transferred amount of energy (Q) results versus mass flow rate.

that the use of twisted tube having higher AR and lower PL in terms of the exergy destruction.

### Second Law Efficiency

The second law efficiency ( $\eta$ ) results belong to the cases considered in the present study is plotted as a function of mass flow rate in Fig. 19. As clearly seen, the case of ETT\_AR=2.0\_PL=50 shows the highest  $\eta$  for all mass flow rates. The highest  $\eta$  was obtained by the case of ETT\_AR=2.0\_PL=50 for mass flow rate of 0.040 kg/s which corresponds to the  $Re$  of 4542 with a value of 0.45, which corresponds to 80% greater than the case of CST. The  $\eta$  results are similar among the non-twisted tubes, while the twisted tubes having higher AR and lower PL show better the  $\eta$ .

In addition to the  $\eta$ , the transferred amount of energy from the tube to the fluid ( $Q$ ) is another significant issue.

For this purpose, Fig. 20 is given to show the result of  $Q$  versus the mass flow rate. General trend of the  $Q$  is similar with that of the  $\eta$ . The highest  $Q$  is obtained as 3564.63 W from the case of ETT\_AR=2.0\_PL=50 at minimum mass flow rate of 0.040 kg/s. Therefore, the use of an elliptical twisted tube in a heat exchanger is a good choice when considering in terms of the second law. Finally, the increase in AR and the decrease in PL provide better  $\eta$  result for all mass flow rate conditions.

### CONCLUSION

The effects of the aspect ratio (AR) and the pitch length (PL) of the elliptical twisted tube (ETT) on the heat exchanger are numerically investigated and determined according to the second law performance. The

findings obtained from the study are summarized as below:

1. The thermal entropy generation decreases with the increment of Reynolds number for all cases. And, the increase in AR and the decrease in PL lead to decrease the thermal entropy generation rate. The lowest thermal entropy generation rate is obtained by the case of ETT\_AR=2.0\_PL=50 as 48.8 W/K, which corresponds to lower than the case of CST as approximately 50% at same mass flow rate.
2. The frictional entropy generation increases with the increment of Reynolds number for all cases. And, the increase in AR and the decrease in PL lead to increase the thermal entropy generation rate. The lowest frictional entropy generation rate is obtained as around of 0.012 W/K at minimum flow rates by almost cases.
3. It is concluded that the thermal entropy generation is more dominant on the total entropy generation compared to the frictional entropy generation. Concisely, the case providing more heat transfer and less fluid friction cause to less total entropy generation rate.
4. The influence of the frictional entropy generation rate on the total entropy generation rate tends to increase with the increment of Reynolds number.
5. The case of ETT\_AR=2.0\_PL=50 is revealed as the most advantageous case according to entropy generation number.
6. Regarding the second law efficiency ( $\eta$ ), as AR increases and PL decreases, higher second law efficiency is obtained for the ETTs. The highest  $\eta$  is obtained as 0.45 by the case of ETT\_AR=2.0\_PL=50 at minimum mass flow rate considered in the study, which corresponds to greater than the case of CST as 80%.
7. Consequently, the use of an elliptical twisted tube having higher aspect ratio and lower twist pitch length is strongly recommended for the heat exchanger applications. However, it should be considered that a twisted tube with a very low pitch length cannot be produced due to deformation on the tube material. A wider range of work including the twist limit can be investigated in future work.

## NOMENCLATURE

AR	aspect ratio of ellipse diameters, nd
Be	Bejan number, nd
$c_p$	specific heat, J/kgK
CST	circular smooth tube
$D_h$	Hydraulic diameter, m
EST	elliptical smooth tube
ETT	elliptical twisted tube
f	friction factor, nd
h	convective heat transfer coefficient, W/m <sup>2</sup> K
k	thermal conductivity, W/mK

L	length of the test tube, m
$N_s$	entropy generation number, nd
Nu	Nusselt number, nd
P	pressure, Pa
PL	twist pitch length of the twisted tube, mm
Pr	Prandtl number, nd
S	entropy, W/K
$q''$	heat flux, W/m <sup>2</sup>
Q	transferred amount of energy, [W]
Re	Reynolds number, nd
T	temperature, K
X	exergy, W
V	velocity, m/s

## Greek symbols

$\rho$	density, kg/m <sup>3</sup>
$\mu$	dynamic viscosity, kg/ms
$\eta$	second law efficiency, nd

## Subscripts

b	bulk
d	destruction
f	frictional
gen	generation
q	imported
s	Refers to surface
th	thermal

## DATA AVAILABILITY STATEMENT

The authors confirm that the data that supports the findings of this study are available within the article. Raw data that support the finding of this study are available from the corresponding author, upon reasonable request.

## CONFLICT OF INTEREST

The author declared no potential conflicts of interest with respect to the research, authorship, and/or publication of this article.

## ETHICS

There are no ethical issues with the publication of this manuscript.

## REFERENCES

- [1] Omidi M, Farhadi M, Jafari M. A comprehensive review on double pipe heat exchangers. *Appl Therm Eng* 2017;110:1075–1090. [\[CrossRef\]](#)

- [2] Jadhav M, Awari R, Bibe D, Bramhane A, Mokashi M. Review on enhancement of heat transfer by active method. *Int J Curr Eng Technol* 2016;1: 221–225.
- [3] Kumar A, Kim M-H. Convective heat transfer enhancement in solar air channels. *Appl Therm Eng* 2015;89:239–261. [\[CrossRef\]](#)
- [4] Afsharpanah F, Sheshpoli AZ, Pakzad K, Ajarostaghi SSM. Numerical investigation of non-uniform heat transfer enhancement in parabolic trough solar collectors using dual modified twisted-tape inserts. *J Therm Eng* 2020;7:133–147. [\[CrossRef\]](#)
- [5] Manglik RM, Bergles AE. Heat transfer and pressure drop correlations for twisted-tape inserts in isothermal tubes: Part II—transition and turbulent flows. *J Heat Transfer* 1993;115:890–896. [\[CrossRef\]](#)
- [6] Eiamsa-ard S, Kiatkittipong K. Heat transfer enhancement by multiple twisted tape inserts and TiO<sub>2</sub>/water nanofluid. *Appl Therm Eng* 2014;70:896–924. [\[CrossRef\]](#)
- [7] Dagdevir T, Ozceyhan V. An experimental study on heat transfer enhancement and flow characteristics of a tube with plain, perforated and dimpled twisted tape inserts. *Int J Therm Sci* 2021;159:106564. [\[CrossRef\]](#)
- [8] Dagdevir T, Uyanik M, Ozceyhan V. The experimental thermal and hydraulic performance analyses for the location of perforations and dimples on the twisted tapes in twisted tape inserted tube. *Int J Therm Sci* 2021;167:107033. [\[CrossRef\]](#)
- [9] Bhakta AK, Singh S N. Thermo-Hydraulic Performance Analysis Of Parabolic Concentrating Solar Water Heater. *J Therm Eng* 2020;6:802–814. [\[CrossRef\]](#)
- [10] Gunes S, Ozceyhan V, Buyukalaca O. Heat transfer enhancement in a tube with equilateral triangle cross sectioned coiled wire inserts. *Exp Therm Fluid Sci* 2010;34:684–691. [\[CrossRef\]](#)
- [11] Keklikcioglu O, Ozceyhan V. Experimental investigation on heat transfer enhancement of a tube with coiled-wire inserts installed with a separation from the tube wall. *Int Commun Heat Mass Transf* 2016;78:88–94. [\[CrossRef\]](#)
- [12] Promvong P. Thermal performance in circular tube fitted with coiled square wires. *Energy Convers Manag* 2008;49:980–987. [\[CrossRef\]](#)
- [13] Yilmaz İH, Mwesigye A, Göksu T. Enhancing the overall thermal performance of a large aperture parabolic trough solar collector using wire coil inserts. *Sustain Energy Technol Assessments* 2020;39:100696. [\[CrossRef\]](#)
- [14] Nanan K, Thianpong C, Promvong P, Eiamsa-ard S. Investigation of heat transfer enhancement by perforated helical twisted-tapes. *Int Commun Heat Mass Transf* 2014;52:106–112. [\[CrossRef\]](#)
- [15] Nanan K, Yongsiri K, Wongcharee K, Thianpong C, Eiamsa-ard S. Heat transfer enhancement by helically twisted tapes inducing co- and counter-swirl flows. *Int Commun Heat Mass Transf* 2013;46:67–73. [\[CrossRef\]](#)
- [16] Keklikcioglu O, Dagdevir T, Ozceyhan V. A CFD based thermo-hydraulic performance analysis in a tube fitted with stepped conical nozzle turbulators. *J Therm Eng* 2016;2:913–940. [\[CrossRef\]](#)
- [17] Dagdevir T, Keklikcioglu O, Ozceyhan V. Heat transfer performance and flow characteristic in enhanced tube with the trapezoidal dimples. *Int Commun Heat Mass Transf* 2019;108:104299. [\[CrossRef\]](#)
- [18] Sabir R, Khan MM, Sheikh NA, Ahad IU, Brabazon D. Assessment of thermo-hydraulic performance of inward dimpled tubes with variation in angular orientations. *Appl Therm Eng* 2020;170:115040. [\[CrossRef\]](#)
- [19] Sheikholeslami M, Gorji-Bandpy M, Ganji DD. Review of heat transfer enhancement methods: Focus on passive methods using swirl flow devices. *Renew Sustain Energy Rev* 2015;49:444–469. [\[CrossRef\]](#)
- [20] Yu C, Zhang H, Wang Y, Zeng M, Gao B. Numerical study on turbulent heat transfer performance of twisted oval tube with different cross sectioned wire coil. *Case Stud Therm Eng* 2020;22:100759. [\[CrossRef\]](#)
- [21] Sheikholeslami M, Gorji-Bandpy M, Ganji DD. Review of heat transfer enhancement methods: Focus on passive methods using swirl flow devices. *Renew Sustain Energy Rev* 2015;49:444–469. [\[CrossRef\]](#)
- [22] Dong X, Jin X, Li P, Bi Q, Gui M, Wang T. Experimental research on heat transfer and flow resistance properties in spiral twisted tube heat exchanger. *Appl Therm Eng* 2020;176:115397. [\[CrossRef\]](#)
- [23] Kanti PK, Sharma KV, Said Z, Gupta M. Experimental investigation on thermo-hydraulic performance of water-based fly ash–Cu hybrid nanofluid flow in a pipe at various inlet fluid temperatures. *Int Commun Heat Mass Transf* 2021;124:105238. [\[CrossRef\]](#)
- [24] Sajid MU, Ali HM. Recent advances in application of nanofluids in heat transfer devices: A critical review. *Renew Sustain Energy Rev* 2019;103:556–592. [\[CrossRef\]](#)
- [25] Dagdevir T, Ozceyhan V. Investigation of the Effect of Using Water Based Hybrid Nanofluid on Thermal and Hydraulic Performance in a Heat Exchanger. *Erciyes Univ J Institue Sci Technol* 2021;37:61–73.
- [26] Keklikcioglu O, Dagdevir T, Ozceyhan V. Heat transfer and pressure drop investigation of graphene nanoplatelet-water and titanium dioxide-water nanofluids in a horizontal tube. *Appl Therm Eng* 2019;162:114256. [\[CrossRef\]](#)

- [27] Verma M, Bansal V, Rana K. Development of passive energy source as earth air pipe heat exchangers (EAPHE) System - A Review. *J Therm Eng* 2020;651–675. [\[CrossRef\]](#)
- [28] Farnam M, Khoshvaght-Aliabadi M, Asadollahzadeh MJ. Heat transfer intensification of agitated U-tube heat exchanger using twisted-tube and twisted-tape as passive techniques. *Chem Eng Process - Process Intensif* 2018;133:137–147. [\[CrossRef\]](#)
- [29] Thantharate, V., & Zodpe DB. Experimental and numerical comparison of heat transfer performance of twisted tube and plain tube heat exchangers. *Int J Sci Eng Res* 2013;4:1107–1113. [\[CrossRef\]](#)
- [30] Wang G, Dbouk T, Wang D, Pei Y, Peng X, Yuan H, et al. Experimental and numerical investigation on hydraulic and thermal performance in the tube-side of helically coiled-twisted trilobal tube heat exchanger. *Int J Therm Sci* 2020;153:106328. [\[CrossRef\]](#)
- [31] Shahsavari A, Bakhshizadeh MA, Arici M, Afrand M, Rostami S. Numerical study of the possibility of improving the hydrothermal performance of an elliptical double-pipe heat exchanger through the simultaneous use of twisted tubes and non-Newtonian nanofluid. *J Therm Anal Calorim* 2021;143:2825–2840. [\[CrossRef\]](#)
- [32] Sun B, Yang A, Yang D. Experimental study on the heat transfer and flow characteristics of nanofluids in the built-in twisted belt external thread tubes. *Int J Heat Mass Transf* 2017;107:712–722. [\[CrossRef\]](#)
- [33] Prattipati R, Narla VK, Pendyala S. Effect of viscosity on entropy generation for laminar flow in helical pipes. *J Therm Eng* 2021:1100–1109. [\[CrossRef\]](#)
- [34] Kumar R, Kumar Verma S. Exergetic And Energetic Evaluation Of An Innovative Solar Air Heating System Coated With Graphene And Copper Oxide Nano-Particles. *J Therm Eng* 2021:447–467. [\[CrossRef\]](#)
- [35] Mburu Zm, Mondal S, Sibanda P, Sharma R. A Numerical Study Of Entropy Generation On Oldroyd-B Nanofluid Flow Past A Riga Plate. *J Therm Eng* 2021:845–866. [\[CrossRef\]](#)
- [36] Mohapatra T, Rout SK. Experimental investigation and performance optimization of a cross flow heat exchanger by entropy generation minimization approach. *J Therm Eng* 2019;5:1–12. [\[CrossRef\]](#)
- [37] Bahiraei M, Mazaheri N, Aliee F. Second law analysis of a hybrid nanofluid in tubes equipped with double twisted tape inserts. *Powder Technol* 2019;345:692–703. [\[CrossRef\]](#)
- [38] Naphon P. Second law analysis on the heat transfer of the horizontal concentric tube heat exchanger. *Int Commun Heat Mass Transf* 2006;33:1029–1041. [\[CrossRef\]](#)
- [39] Sadighi Dizaji H, Khalilarya S, Jafarmadar S, Hashemian M, Khezri M. A comprehensive second law analysis for tube-in-tube helically coiled heat exchangers. *Exp Therm Fluid Sci* 2016;76:118–125. [\[CrossRef\]](#)
- [40] Khanmohammadi S, Mazaheri N. Second law analysis and multi-criteria optimization of turbulent heat transfer in a tube with inserted single and double twisted tape. *Int J Therm Sci* 2019;145:105998. [\[CrossRef\]](#)
- [41] Sheikholeslami M, Jafaryar M, Shafee A, Li Z. Investigation of second law and hydrothermal behavior of nanofluid through a tube using passive methods. *J Mol Liq* 2018;269:407–416. [\[CrossRef\]](#)
- [42] Mwesigye A, Huan Z, Meyer JP. Thermal performance and entropy generation analysis of a high concentration ratio parabolic trough solar collector with Cu-Therminol®/VP-1 nanofluid. *Energy Convers Manag* 2016;120:449–465. [\[CrossRef\]](#)
- [43] Ibrahim M, Saeed T, Bani FR, Sedeh SN, Chu Y-M, Toghraie D. Two-phase analysis of heat transfer and entropy generation of water-based magnetite nanofluid flow in a circular microtube with twisted porous blocks under a uniform magnetic field. *Powder Technol* 2021;384:522–541. [\[CrossRef\]](#)
- [44] Cengel YA, John CM. *Fluid Mechanics: Fundamentals and Applications*. New York: MC Graw-Hill Education, 2012.
- [45] Aly WIA. Numerical study on turbulent heat transfer and pressure drop of nanofluid in coiled tube-in-tube heat exchangers. *Energy Convers Manag* 2014;79:304–316. [\[CrossRef\]](#)
- [46] Elsayed A, Al-dadah RK, Mahmoud S, Rezk A. Numerical investigation of turbulent flow heat transfer and pressure drop of AL<sub>2</sub>O<sub>3</sub>/water nanofluid in helically coiled tubes. *Int J Low-Carbon Technol* 2015;10:275–282. [\[CrossRef\]](#)
- [47] Bas H, Ozceyhan V. Heat transfer enhancement in a tube with twisted tape inserts placed separately from the tube wall. *Exp Therm Fluid Sci* 2012;41:51–58. [\[CrossRef\]](#)
- [48] Pourdel H, Afrouzi HH, Akbari OA, Miansari M, Toghraie D, Marzban A, et al. Numerical investigation of turbulent flow and heat transfer in flat tube. *J Therm Anal Calorim* 2019;135:3471–3483. [\[CrossRef\]](#)
- [49] Guo J, Xu M, Cheng L. Numerical investigations of circular tube fitted with helical screw-tape inserts from the viewpoint of field synergy principle. *Chem Eng Process Process Intensif* 2010;49:410–417. [\[CrossRef\]](#)
- [50] Saysroy A, Changcharoen W, Eiamsa-ard S. Performance assessment of tubular heat exchanger tubes containing rectangular-cut twisted tapes with alternate axes. *J Mech Sci Technol* 2018;32:433–445. [\[CrossRef\]](#)
- [51] Fluent. *ANSYS Fluent User Guide* 2016.

- [52] Cengel YA, Boles MA. Thermodynamics: an Engineering Approach. 5th ed. Boston: McGraw-Hill Higher Education; 2008.
- [53] Bejan A. Thermodynamic optimization of geometry in engineering flow systems. *Exergy, An Int J* 2001;1:269–277. [[CrossRef](#)]
- [54] Gnielinski V. New equations for heat and mass transfer in turbulent pipe and channel flow. *Int Chem Eng* 1976;27:359–368.
- [55] Blasius H. Das Aehnlichkeitsgesetz bei Reibungsvorgängen in Flüssigkeiten. *Mitt Forschungsarbeiten Gebiete Ingenieurwesens* 1913;131:1–41. [[CrossRef](#)]